International Journal of Heat and Mass Transfer 52 (2009) 3963–3971

Contents lists available at ScienceDirect

International Journal of Heat and Mass Transfer

journal homepage: www.elsevier.com/locate/ijhmt

Heat transfer of gas–liquid mixture in micro-channel heat sink

G. Hetsroni *, A. Mosyak, E. Pogrebnyak, Z. Segal

Department of Mechanical Engineering, Technion – Israel Institute of Technology, 32000 Haifa, Israel

ARTICLE INFO

Article history:
Received 12 January 2009
Accepted 23 March 2009
Available online 4 May 2009

Keywords:
Heat-transfer
Gas-liquid
Micro-channel

ABSTRACT

The main objective of the present investigation is to study heat transfer in parallel micro-channels of 0.1 mm in size. Comparison of the results of this study to the ones obtained for two-phase flow in "conventional" size channels provides information on the complex phenomena associated with heat transfer in micro-channel heat sinks. Two-phase flow in parallel micro-channels, feeding from a common manifold shows that different flow patterns occur simultaneously in the different micro-channels: liquid alone (or single-phase flow), bubbly flow, slug flow, and annular flow (gas core with a thin liquid film, and a gas core with a thick liquid film). Although the gas core may occupy almost the entire cross-section of the triangular channel, making the side walls partially dry, the liquid phase always remained continuous due to the liquid, which is drawn into the triangular corners by surface tension. With increasing superficial gas velocity, a gas core with a thin liquid film is observed. The visual observation showed that as the air velocity increased, the liquid droplets entrained in the gas core disappeared such that the flow became annular. The probability of appearance of different flow patterns should be taken into account for developing flow pattern maps. The dependence of the Nusselt number, on liquid and gas Reynolds numbers, based on liquid and gas superficial velocity, respectively, was determined in the range of Re_{LS} = 4–56 and Re_{GS} = 4.7–270. It was shown that an increase in the superficial liquid velocity involves an increase in heat transfer (Nu_L). This effect is reduced with increasing superficial gas velocity, in contrast to the results reported on two-phase heat transfer in "conventional size" channels.

1. Introduction

Gas–liquid flows occur widely in both nature and industrial applications, including energy production (e.g., oil transportation, steam generators, cooling systems) and chemical engineering (e.g., bubble columns, reactors, aeration systems). Two-phase flows in micro-channels have attracted attention because their wide applicability to such advanced fields as MEMS, electronic cooling, medical and genetic engineering, bioengineering, etc. At present, additional knowledge of flow and heat transfer in micro-scale flow passages of a size less than 100 μm is required. Specifically, fundamental knowledge of two-phase flow characteristics in small flow passages, such as the flow pattern, void fraction, pressure drop, and heat transfer coefficient, is crucial for engineering design purposes as well as for evaluation of practical performance.

Papers by Ghiaasiaan and Abdel-Khalik [1], Serizawa et al. [2], Kawahara et al. [3], Garimella and Sobhan [4], Celata [5], and Cheng and Wu [6] extensively reviewed the literature on two-phase flow pattern in micro-channels. However, our current knowledge on two-phase flow characteristics and heat transfer in parallel micro-channels is still limited and in reality the literature sources are sparse. One of the questions is whether the two-phase heat transfer coefficient in micro-channels is different from that encountered in "conventional" size channels. Most of the heat transfer correlations are based on data obtained in flow boiling from relatively large diameter conduits and the predictions from these correlations show considerable variability. Effects of superficial liquid and gas velocity on heat transfer in gas–liquid flow and its connection to flow characteristics were studied by Hetsroni et al. [7–9], Kim et al. [10], Bao et al. [11], Ghajar et al. [12], and Zimmerman et al. [13]. These researches were carried out for "conventional size" tubes of d = 1.95–42 mm.

The main objective of the present investigation is to study the flow pattern, pressure drop and heat transfer in parallel micro-channels of a size about 0.1 mm. A comparison of results of this study with ones obtained for two-phase flow in "conventional" size channels provides information for understanding the complex phenomena associated with two-phase gas–liquid flow in micro-channel heat sinks.

2. Experimental set-up and procedure

2.1. Experimental facility

The experimental facility and flow loop were described in detail by Hetsroni et al. [14]. The loop consists of a liquid pump, piping, test module, entrance and exit tanks. Deionized water and air were

* Corresponding author. Tel.: +972 48 292058; fax: + 972 48 238101.
E-mail address: hetsroni@tx.technion.ac.il (G. Hetsroni).

0017-9310/$ - see front matter © 2009 Elsevier Ltd. All rights reserved.
doi:10.1016/j.ijheatmasstransfer.2009.03.027

Nomenclature

A	overall cross-section of micro-channels
C	constant of friction multiplier
d	diameter
F	area of heater
h	heat transfer coefficient
k	thermal conductivity
m	mass flux
N	electric power
Nu	Nusselt number
q	heat flux
Q	volumetric flow rate
Re	Reynolds number
T	temperature
U	velocity
X	Lockhart–Martinelli parameter

Greek symbols

α	void fraction
$\alpha(c)$	void fraction for bubble core and gas core with a thick liquid film
β	homogeneous void fraction
ΔP	pressure drop
ρ	fluid density
Φ	friction multiplier
τ	time
ν	kinematic viscosity

Subscripts

ac	acceleration
cal	calculated
con	contraction
ex	experimental
G	gas
GS	superficial gas
h	hydraulic, heated perimeter
in	inlet
L	liquid
LS	superficial liquid
Mean	mean
Mix	mixture
Out	outlet
TP	two-phase
w	wall

used in this study. The working mixture was pumped from the entrance tank through the inlet collector to the micro-channels in the test module, and from the micro-channels through the outlet collector to the exit tank. The two-phase flow was achieved by the introducing water and air into a mixer as shown in Fig. 1. The experiments were performed in an open loop, therefore the outlet pressure was close to atmospheric. Two types of pumps were used: peristaltic pump and mini gear pump.

The temperature of the working fluid was measured at the inlet and outlet collectors of the test module, by 0.3 mm type-T thermocouples. The thermocouples were calibrated in 0.1 K increments. The flow rate of the working fluid was measured by a weighting method. Pressures were measured at the inlet and the outlet manifolds of the test module by silicon pressure sensors, with sensitivity of 3.3 mV/kPa, and response time 1.0 ms. Data were collected by a data acquisition system.

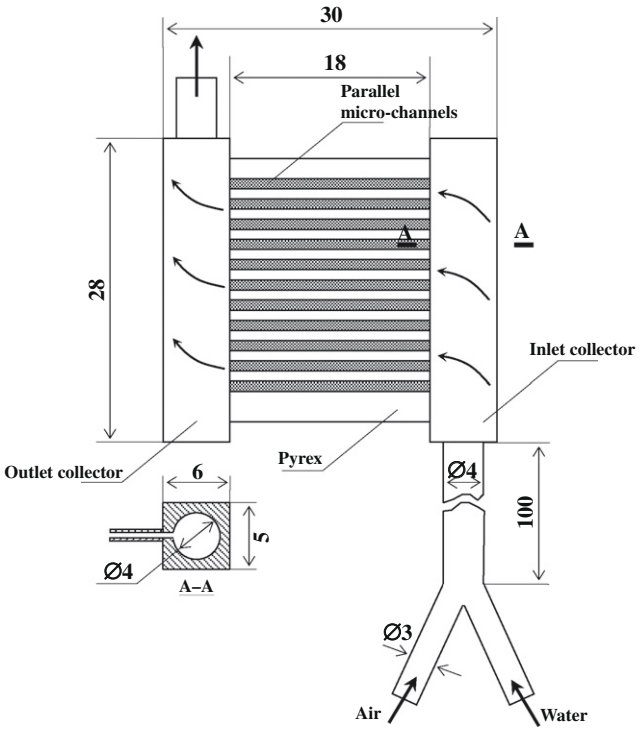

Fig. 1. Experimental facility. All dimensions in [mm].

The test module is shown in Fig. 2. It was fabricated of a square-shape silicon substrate 15 × 15 mm, 530 μm thick, covered by a Pyrex cover, 500 μm thick, which served both an insulator and a transparent cover through which flow in the micro-channels could be observed. The Pyrex cover was anodicaly bonded to the silicon chip, in order to seal the channels. In the silicon substrate, parallel micro-channels were etched, the cross-section of each channel was an isosceles triangle. The angles at the base were 55°. We used the test module having 21 micro-channels with hydraulic diameter of 130 μm. An electrical heater of 10 × 10 mm^2, was deposited on the back surface of the silicon, and served to simulate the heat source. The heater was coated with a thin layer of black diffusive paint, with emissivity $\varepsilon \approx 0.96$. The heater had a serpentine pattern and a dimension of 0.001 mm in thickness, 0.2 mm in width and 250 mm in length. This design allowed a uniform heating of the surface and reduces the contact resistance between the heater and the wafer. The input voltage and current were controlled by a power supply.

2.2. Flow and thermal visualization

A microscope with an additional camera joint was assembled to connect a high-speed camera to the microscope. A high-speed camera with a maximum frame rate of 10,000 fps, was used to visualize the two-phase flow regimes in the micro-channels. To study the temperature field of the resistor a high-speed focal plane array radiometer containing 75 kpixels was utilized. The measurement resolution was 0.03 °C with a standard measurement accuracy of ±2 °C for the range of 0–100 °C and ±2% above 100 °C. In an isolated laboratory environment using an appropriate black body, improved calibration and non-uniformity-correction are possible, therefore an accuracy of ±1 K can be achieved. Using microscopic lens and reduced array size, IR measurements can be taken at up to 800 Hz with a 30 μm spatial resolution.

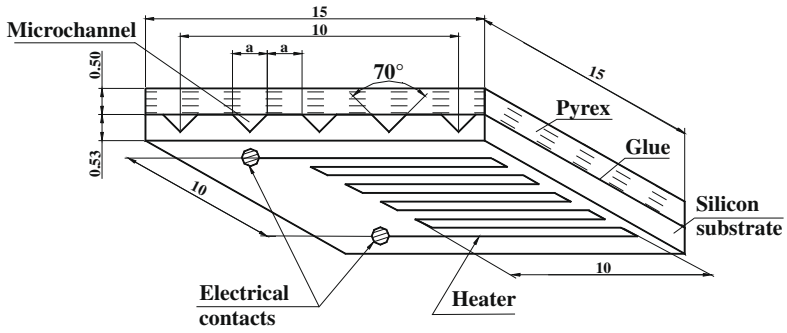

Fig. 2. Test module. All dimensions in [mm].

2.3. Data reduction

The parameters used in the data reduction and analyses are summarized below:

Probability of appearance of different flow patterns. In the parallel channels having common inlet and outlet collectors, non-uniform distribution of the working fluid occurs. We observed simultaneous different flow patterns in different parallel micro-channels and also alternate flow patterns in a given micro-channel. This point is illustrated in Figs. 3 and 4. In these figures four parallel channels of the test module can be seen with the flow from left to right. The field of view is 2.4 mm in the streamwise direction and 2.2 mm in the spanwise direction. At flow conditions of the present study, different flow patterns were observed. These can be classified depending on the interfacial configuration: liquid alone (or single-phase flow), L; bubbly flow, B; slug flow, S; and semi-annular flow (gas core with a thin liquid film, A1, gas core with a thick liquid film, A2).

Bubbly flow is characterized by the appearance of distinct non-spherical bubbles, generally elongated in the streamwise direction of the triangular channel. This flow pattern was also observed by Triplett et al. [15] in the 1.097 mm diameter circular tube, and by Zhao and Bi [16] in the triangular channel of $d_h = 0.866$ mm. This flow, referred to by Zhao and Bi [16] as "capillary bubbly flow", has the following characteristics (as seen from Fig. 3): the gas bubbles are regularly distributed in the liquid phase, represented by a train of bubbles, essentially ellipsoidal in shape, spanning almost the entire cross-section with their centers located along the center line of the channel. The flow with elongated cylindrical bubbles may be referred to "slug" flow, Fig. 4a. It is seen from this figure that a liquid film is formed on the side walls of the channel with a continuous gas core, which contains some liquid droplets. The flow with a continuous gas core that occupies almost the entire cross-section was referred to the gas core with a thin liquid film. In this case the high-speed core gas entrains the liquid phase, such flow pattern was also observed by Serizawa et al. [2]. No stratified flow occurred in micro-channels as reported in previous studies of two-phase flow patterns in channels with a diameter close to 1 mm (Triplett et al. [15]; Zhao and Bi [16]; Damianides and Westwater [17]; Fukano and Kariyasaki [18]). It should be noted that although the gas core may occupy almost the entire cross-section of the triangular channel, making the side walls partially dry, the liquid phase always remained continuous due to the fact that the liquid is drawn into the triangular corners by surface tension.

In developing a two-phase flow pattern map it became clear that flow patterns need to be defined as to fully describe the flow characteristics, due to simultaneous occurrence of different flow patterns in the channel under any given flow conditions. Thus, the time fractions of different flow patterns were obtained for each two-phase flow condition. The number of images containing each

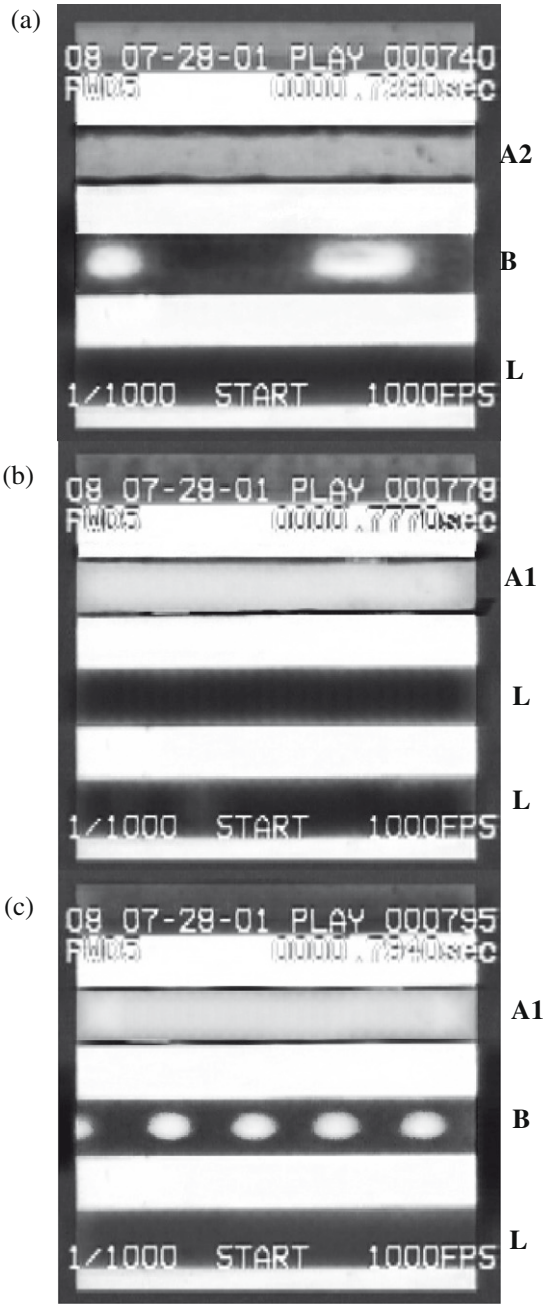

Fig. 3. Flow patterns at different time. $U_{GS} = 15$ m/s, $U_{LS} = 0.15$ m/s. (a) $\tau = 0.7320$ s, (b) $\tau = 0.7770$ s, (c) $\tau = 0.7940$ s. L, single-phase liquid; B, bubbly flow; A1, gas core with thin liquid film; A2, gas core with thick liquid film.

Fig. 4. Flow patterns at different time. U_{GS} = 0.49 m/s, U_{LS} = 0.061 m/s. (a) τ = 1.084 s, (b) τ = 1.540 s, (c) τ = 5.078 s. L, single-phase liquid; S, slug flow; A1, gas core with thin liquid film; A2, gas core with thick liquid film.

flow pattern was then counted and the probability of appearance was computed for a given flow condition. Based on these probabilities the time-averaged void fraction for each flow condition was defined.

Void fraction. The method is based on analyzing the images of gas–liquid interfaces recorded in the observation window of the channel (Triplett et al. [19]; Serizawa et al. [2]; Kawahara et al. [3]). Void fraction in the present study was estimated by the method suggested by Kawahara et al. [3]): analyzing the images of gas–liquid interfaces recorded in the observation window of the channel. Each image covered a distance of about 1 mm in the flow direction.

For the flow pattern, L, that contains liquid alone, the void fraction, was assumed to be zero, $\alpha = 0$. For gas core with a thin liquid film, A1, the void fraction was estimated as $\alpha = 1$. For bubbly flow, B; slug flow, S; and gas core with a thick liquid film, A2, the void fraction was assumed to be between zero and unity, $0 < \alpha(c) < 1$, and was estimated by the regarding the gas core as a cylinder of a smaller diameter, $d(c)$, than the channel hydraulic diameter, d_h, i.e., $\alpha(c) = d(c)/d_h$. By counting the number of images containing each flow type, the probability of appearance of different flow patterns was taken into account. Then, the void fraction was determined:

$$\alpha = \left(N(\mathrm{A1}) + \sum \alpha(c)\right)\Big/N, \tag{1}$$

where N(A1) is the number of images with a thin liquid film, $\alpha(c)$ was summed for all the images containing bubbly flow, slug flow, and gas core with a thick liquid film, N is the total number of images counted.

Pressure drop. The overall pressure drop measured in horizontal two-phase flow is given by

$$\Delta P = \Delta P_{TP} + \Delta P_{con} + \Delta P_{ac}, \tag{2}$$

where ΔP_{TP} is the pressure drop due to wall friction, ΔP_{con} is the pressure loss due to contractions from the inlet manifold to the micro-channels and from the micro-channels to the outlet manifold, ΔP_{ac} is the pressure change due to acceleration. ΔP_{con} and ΔP_{ac} were estimated from relations recommended in some references (e.g., Kawahara et al. [3]).

Heat flux. In order to determine the heat flux from the heater to the working fluid, the heat losses due to conduction, convection and radiation were taken into account. There are several heat transfer surface areas that may be used in the calculations. The first is the plate area of the heater $F = 1 \times 1$ cm^2. The second, F_h, can be defined relative to the mean heat flux along the heated perimeter. In this study $F = F_h$, and the heat transferred to the fluid was defined as

$$q = \varphi N/F_h, \tag{3}$$

where φ is the ratio of the heat transferred to the working fluid to the local heat generation, and N is the electric power applied to the heater. The values of φ were in the range of 0.8–0.9 depending on flow rate and heat flux.

Mass flux. The mass flux, m, at the inlet of the test section for air and water was calculated as

$$m = Q\rho/A, \tag{4}$$

where A is the overall cross-section of the micro-channels, Q is the volumetric flow rate, and ρ is the fluid density, for air and water, respectively.

Heat transfer coefficient. The heat transfer coefficient in the boiling regime, assuming thermal equilibrium, is given by:

$$h = q/\left(T_{w,mean} - T_{mix,mean}\right), \tag{5}$$

where h is the heat transfer coefficient, $T_{w,mean}$ is the average temperature at the channel wall where saturated boiling occurs, $T_{mix,mean}$ is the average mixture temperature calculated as:

$$T_{w,mean} = 0.5\left(T_{mix,in} + T_{mix,out}\right), \tag{6}$$

where $T_{mix,in}$ and $T_{mix,out}$ are the temperatures of the air–water mixture measured at the inlet and the outlet manifolds of the test module.

2.4. Experimental uncertainty

An estimation of an error measurement of wall temperature was obtained according to the standard 1995 Guide to the Expression of Uncertainty of the Measurements [20]. The details of calculation are presented by Hetsroni et al. [21]. The error in

determining the heat transfer coefficient was calculated from an estimation of the errors that affect the measurements of the following quantities: heat flux and the average temperature difference between the heater and the saturation temperature.

The error in determining the power generated by Joule heating is due to errors of measurements of both the electric current and the electric resistance. The error in estimation of the heat losses is due to correlations for calculation of natural convection and radiation heat transfer. The experimental runs were repeated and the average values obtained from the measurements are discussed below. The uncertainties in determining various parameters in this study are given in Table 1.

3. Results

3.1. Void fraction

In Fig. 5 the void fraction, α, is plotted versus the homogeneous void fraction, β. The open symbols represent adiabatic flow, the closed symbols represent two-phase flow in the range of heat flux $q = 4.5–14.4\ \mathrm{W/cm^2}$. The majority experiments were conducted at of the. $\alpha > 0.8$. The solid line shows the correlation obtained by Kawahara et al. [3].

$$\alpha = \frac{0.03\beta^{0.5}}{1 - 0.97\beta^{0.5}}. \tag{7}$$

The data and best-fit curve are highly non-linear indicating strong deviations from linear relations for a homogeneous flow. For the latter, Ali et al. [22] have reported that the void fraction in narrow channels with $d_h \sim 1$ mm can be approximately given by an Armand-type [23] correlation, $\alpha = 0.8\beta$, which is shown by a dashed line in Fig. 5. On the other hand, in the study by Serizawa et al. [2] the cross-sectional averaged void fraction was correlated with the Armand [23] correlation.

Disagreement between the results of void fraction in micro-channels obtained by different investigators, was discussed by Ide et al. [24]. They addressed the differences in gas–liquid two-phase flow characteristics that occur in conventional size channels and micro-channels by examining the two-phase flow pattern, interfacial wave, void fraction and friction pressure drop data obtained in circular and rectangular channels with a hydraulic diameter ranging from 50 μm to 6.0 mm. Two different inlet sections were covered in micro-channel experiments, a gradually reducing section and a T-junction. The void fraction data obtained in micro-channels and conventional size channels showed significant differences depending on the channel cross-section and inlet geometry. For the micro-channel with a diameter of 100 μm, the effects of the inlet geometry and gas–liquid mixing method on the void fraction were seen to be quite strong, while the conventional size channels have shown a much smaller effect of inlet geometry on the void fraction.

Table 1
Experimental uncertainty.

No.	Source of uncertainty	Symbol	Uncertainty (%)
1	Hydraulic diameter	d_h	2
2	Heat flux	q	4–6
3	Superficial liquid velocity	U_{LS}	2–3
4	Superficial gas velocity	U_{GS}	4–12
5	Void faction	α	8–20
6	Pressure drop	ΔP	4–7
7	Heat transfer coefficient	h	14–16
8	Nusselt number	Nu_L	16–18
9	Reynolds number of water	Re_L	4–6
10	Reynolds number of air	Re_G	5–14

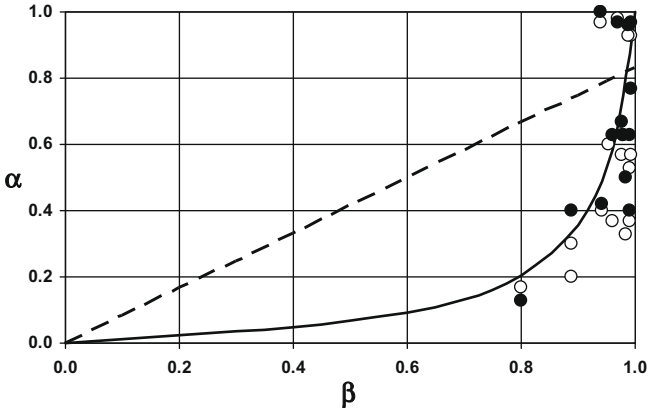

Fig. 5. Void fraction: •, adiabatic flow; ○, diabatic flow; —, Kawahara et al. [3]; - - Armand [23].

The void fraction data obtained with a T-junction inlet showed a linear relationship between the void fraction and volumetric quality, in agreement with the homogeneous flow model predictions. In contrast, the void fraction data from the reducing section inlet experiments by Kawahara et al. [3] showed a non-linear void fraction-to-volumetric quality relationship. This trend implies a strong departure from homogeneous flow and indicates a large slip between the liquid and gas phases. Kawahara et al. [3] observed mainly long gas core flows surrounded by thin, thick and wavy liquid films, which likely moved with a much slower velocity due to a large viscous effect near the channel wall. They observed few plug flows with short gas plugs for the same micro-channel connected to a reducer inlet. Our results agree with observations reported by Kawahara et al. [3]. From these data, it is clear that the void fraction in a micro-channel strongly depends on the inlet geometry and gas–liquid mixing method due to the significantly different flow patterns that occur in the micro-channel. Thus, similar void fraction data can be obtained in micro-channels and conventional size channels, but the micro-channel void fraction is sensitive to the inlet geometry and deviates significantly from the Armand [23] correlation.

3.2. Flow regime map

Experimental data on flow patterns and the transition boundaries are usually mapped on a two-dimensional plot. Two basic types of coordinates may be used for the flow regime maps – one that uses dimensional coordinates such as superficial velocities, and another that uses some kind of dimensionless group. Dimensionless analysis is the straightforward approach to select the proper dimensionless coordinates. The flow pattern transition boundaries should be a function of all these variables. Maps based on dimensionless coordinates are more general, for example, they should be independent of fluid properties and channel size. Unfortunately, determining the correct dimensionless coordinates for flow pattern is not at all trivial. Moreover, there is no guarantee that two dimensionless coordinates are sufficient in the majority of cases. The maps obtained for a given geometry and channel size are usually based on superficial liquid and gas velocities. The usual experimental approach is to apply these variables to all transitions in all channels, assuming that entrance effects, channel geometry and size, roughness, solid–liquid–gas contact wetting angle, etc., have no influence on flow pattern. The chance of this approach being correct, outside the specific range of operating conditions that has been used to correlate the data, is very slim.

The range of superficial liquid and gas velocities covered in the present study is shown in Figs. 6 and 7 as shaded rectangular area.

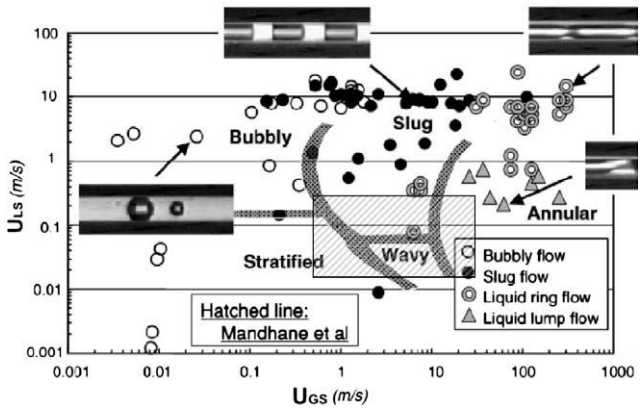

Fig. 6. Flow pattern map for air–water flow in 20 μm tube. (Reprinted from Serizawa et al. [2] with permission) The shaded rectangular area shows parameters of the present study.

Fig. 6 shows a flow pattern map obtained for air–water two-phase flow in a 20 μm silica tube by Serizawa et al. [2] at nearly atmospheric pressure. The two-phase flow patterns are different from those observed by Serizawa et al. [2]. We did not observe stratified and wavy flow.

Fig. 7 shows the overall two-phase flow regime map developed for micro-channels by Kawahara et al. [3]. The lines represent the boundaries at which flow regime transition occurred among the four flow patterns, i.e., slug–ring, ring–slug, multiple and semi-annular flows. According to the classification given by Kawahara et al. (2002) semi-annular flow is the one in which the flow alternates mostly between A1 and A2 regime and the time-averaged void fraction is greater than 0.8. The present experiments were carried out under this condition.

3.3. Frictional pressure drop

The results are presented in Table 2.

Homogeneous model. The homogeneous mixture model is the simplest method for calculating the frictional two-phase pressure drop.

The two-phase frictional pressure gradient is obtained from:

$$\left(-\frac{dP}{dz}\right)_{TP} = \Phi_L^2 \left(-\frac{dP}{dz}\right)_L, \tag{8}$$

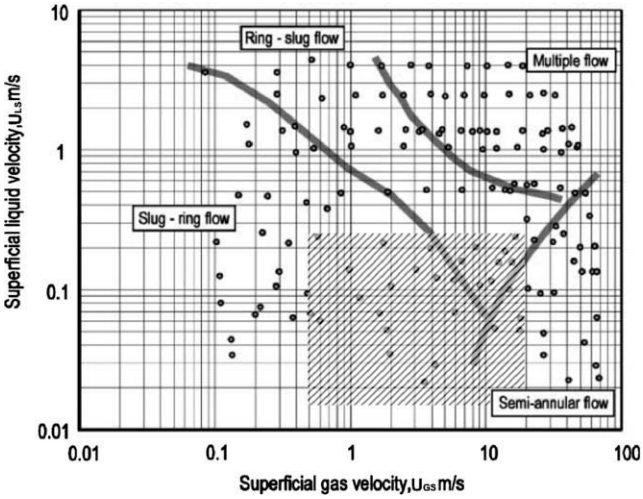

Fig. 7. Two-phase flow pattern map for air–water flow in 100 μm micro-channel. (Reprinted from Kawahara et al. [3] with permission) The shaded rectangular area shows parameters of the present study.

Table 2
Pressure drop data.

U_{GS}	U_{LS}	Φ^2		ΔP (Pa)		
(m/s)	(m/s)	$C = 0.66$	$C = 0.24$	$C = 0.66$	$C = 0.24$	ΔP_{exp}
0.49	0.031	1.497	1.170	359.5	280.8	270
0.49	0.061	1.370	1.190	679.1	590.2	630
0.49	0.12	1.292	1.209	1328.1	1242.9	1300
0.49	0.24	1.254	1.225	2578.9	2518.9	2600
1.4	0.015	2.148	1.114	241.4	125.3	140
1.4	0.031	1.793	1.138	430.5	273.3	300
1.4	0.061	1.564	1.161	775.7	575.7	550
1.4	0.12	1.412	1.183	1451.5	1215.7	1300
1.4	0.24	1.320	1.201	2714.1	2469.6	2500
2.4	0.015	2.440	1.100	274.3	123.7	120
2.4	0.031	1.991	1.124	478.0	269.8	260
2.4	0.061	1.699	1.147	842.2	568.6	640
2.4	0.12	1.500	1.169	1542.1	1202.0	1350
2.4	0.24	1.376	1.189	2828.7	2444.7	1400
5.4	0.015	3.307	1.073	371.8	120.7	130
5.4	0.031	2.581	1.094	619.8	262.8	310
5.4	0.061	2.105	1.117	1043.7	553.7	590
5.4	0.12	1.775	1.140	1824.9	1171.7	1100
5.4	0.24	1.561	1.162	3208.3	2388.1	2300
29	0.015	6.381	1.038	717.4	116.7	120
29	0.031	4.682	1.052	1124.3	252.5	250
29	0.061	3.564	1.068	1766.9	529.5	570
29	0.12	2.783	1.087	2860.3	1117.8	1240
29	0.24	2.264	1.108	4654.6	2278.2	2460

where $(-dP/dz)_L$ represents the frictional pressure gradient when all fluid is assumed to be liquid. The Lockhart and Martinelli [25] correlation uses a two-phase friction multiplier, defined by Eq. (8). The friction multiplier has been correlated in terms of the Lockhart–Martinelli [25] parameter, X, given by

$$X^2 = \frac{(\Delta P/\Delta z)_L}{(\Delta P/\Delta z)_G}, \tag{9}$$

where $(\Delta P/\Delta z)_G$ is the frictional pressure drop when the gas is assumed to flow alone in the channel. A widely used correlation to calculate the friction multiplier is that proposed by Chisholm [26] for conventional size channels

$$\Phi^2 = 1 + \frac{C}{X} + \frac{1}{X^2}, \tag{10}$$

where C, is a constant. The value of $C = 0.66$ was given by Mishima and Hibiki [27]. We found that $C = 0.24$ was best fit the two-phase pressure drop measured by Kawahara et al. [3] in a circular tube of $d = 100$ μm.

A comparison of the two-phase frictional pressure gradient data with the predictions of the Lockhart–Martinelli correlation using different C-values is shown in Fig. 8a,b, including $C = 0.24$ and $C = 0.66$. A good agreement (within ±10%) was obtained with the use of the value of $C = 0.24$. As can be seen (Fig. 8b) agreement with he use of the value of $C = 0.66$ is not good.

3.4. Heat transfer

Results are presented in Table 3. Fig. 9 shows the dependence of the Nusselt number, Nu_L, based on liquid thermal conductivity and Reynolds number, Re_{GS}, based on superficial gas velocity and kinematic gas viscosity. As shown in Fig. 9 an increase in superficial liquid velocity involves an increase in heat transfer (Nu_L). This effect falls off with increasing superficial gas velocity in the range $Re_{GS} = 4.7–270$.

Fig. 10a–e illustrates the effect of Re_{GS} on heat transfer depending on Re_{LS}. In the range of $Re_{LS} = 4–56$ heat transfer decreases with increasing Re_{GS}.

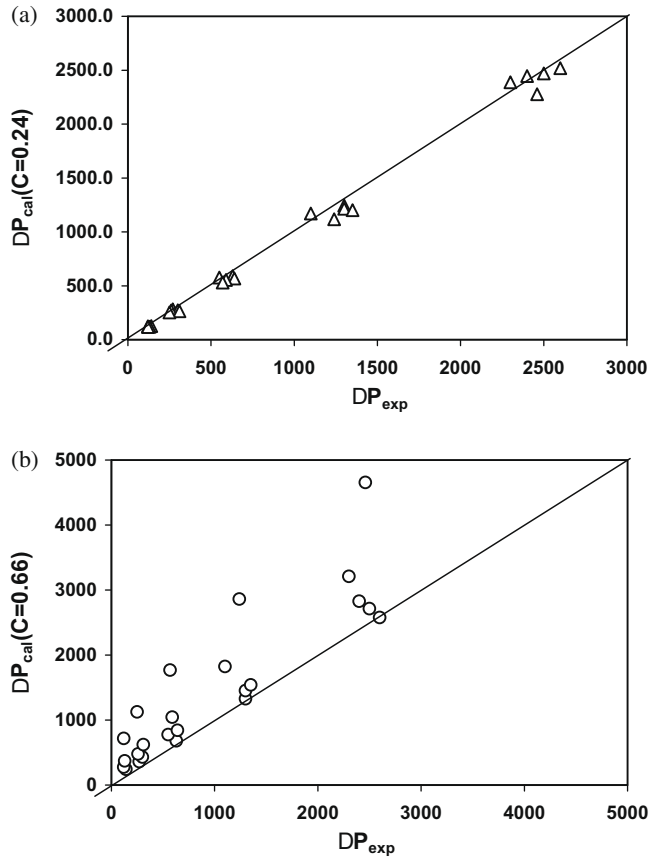

Fig. 8. Comparison of the experimental two-phase frictional pressure gradient data with predictions of the Lockhart–Martinelli correlation. (a) △, $C = 0.24$; (b) ○, $C = 0.66$.

The Nusselt number may be calculated as:

$$Nu_L = 0.044 Re_{LS}^{0.96} Re_{GS}^{-0.18} \quad \text{for} \quad Re_{GS} = 4.7 - 270, Re_{LS} = 4.0 - 8.0 \tag{11}$$

$$Nu_L = 0.13 Re_{LS}^{0.96} Re_{GS}^{-0.40} \quad \text{for} \quad Re_{GS} = 4.7 - 270, Re_{LS} = 8.0 - 56, \tag{12}$$

Table 3
Heat transfer in two-phase flow.

Re_{GS}	Re_{LS}	$Nu_{tp,exp}$	$Nu_{tp,cal}$	$Nu_{tp}/Nu_{L,exp}$
4.7	8	0.20	0.25	0.91
4.7	15	1.20	0.94	0.86
4.7	28	1.70	1.70	0.89
4.7	56	3.00	3.30	0.97
14	4	0.08	0.10	0.8
14	8	0.18	0.20	0.82
14	15	0.61	0.61	0.43
14	28	1.20	1.10	0.75
14	56	2.30	2.20	0.79
26	4	0.10	0.09	1
26	8	0.20	0.18	0.91
26	15	0.51	0.41	0.36
26	28	0.90	0.86	0.47
26	56	1.50	1.70	0.52
51	4	0.10	0.08	1
51	8	0.18	0.16	0.82
51	15	0.33	0.37	0.24
51	28	0.62	0.66	0.33
51	56	1.30	1.30	0.45
270	4	0.05	0.06	0.5
270	8	0.11	0.12	0.5
270	15	0.18	0.19	0.13
270	28	0.33	0.35	0.17
270	56	0.58	0.68	0.2

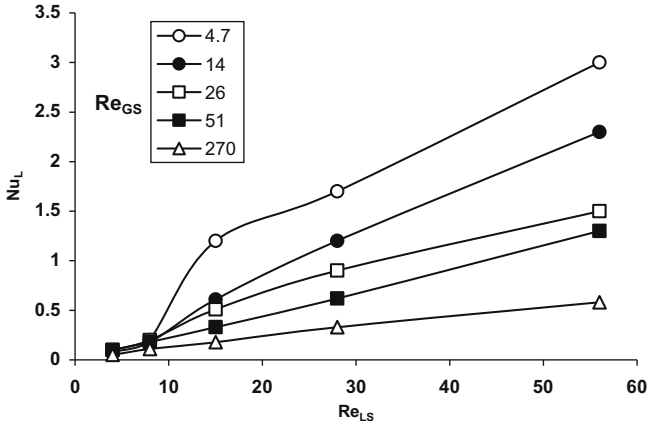

Fig. 9. Effect of superficial liquid velocity on heat transfer in parallel triangular micro-channels of $d_h = 130$ μm.

where $Nu_L = hd_h/k_L, Re_{LS} = U_{LS}d_h/v_L, Re_{GS} = U_{GS}d_h/v_G$, h is the heat transfer coefficient, k_L is the liquid thermal conductivity, U_{LS} and U_{GS} are the liquid and gas superficial velocities, respectively, and v_L and v_G are the liquid and gas kinematic viscosity, respectively. Fig. 11 shows the comparison of experimental Nusselt numbers to predictions by Eqs. (11) and (12).

Flow patterns and heat transfer were investigated by Ghajar et al. [12] in slug and annular flow in a 25 mm horizontal tube. The results presented clearly show that two-phase mean heat transfer coefficients are strongly influenced by the liquid superficial Reynolds number (Re_{LS}), and the heat transfer coefficient increases nearly proportionally as Re_{LS} increases. These observations are in agreement with our results obtained in micro-channels with hydraulic diameter of 130 μm.

Ghajar et al. [12] also reported that the effect of superficial gas velocity on heat transfer depended on flow pattern and showed its own distinguished trend. In the range of $Re_{GS} = 800–1800$ heat transfer coefficient increases with increasing Re_{GS}. Bao et al. [11] also reported that the measured heat transfer coefficients for the air–water system are always higher than would be expected for the corresponding single-phase liquid flow, so that the addition of air can be considered to have an enhancing effect. This paper reports an experimental study of non-boiling air–water flows in a narrow horizontal tube (diameter 1.95 mm). Results are presented for pressure drop characteristics and for local heat transfer coefficients over a wide range of gas superficial velocity (0.1–50 m/s), liquid superficial velocity (0.08–0.5 m/s) and wall heat flux (3–58 kW/m^2). From Eqs. (11) and (12) one may conclude that for micro-channels of $d_h = 130$ μm in the range of $Re_{LS} = 4–56$ and $Re_{GS} = 4.7–270$ an increase in Re_{GS} leads to a decrease in the heat transfer coefficient as opposed to results [11,12] reported for the channels of 1.95–25 mm.

4. Conclusions

In large tubes, as well as in tubes of a few millimeters in diameter, two-phase flow patterns are, in general, dominated by gravity with minor surface tension effects. In micro-channels with diameters on the order of a few microns to a few hundred microns, two-phase flow is influenced mainly by surface tension, visco's and inertia forces. The stratified flow patterns commonly encountered in single macro-channels were not observed in single micro-channels.

The micro-channels are sensitive not only to inlet geometry but also to the method of gas–liquid injection.

Two-phase flow in parallel micro-channels, feeding from a common manifold, shows that different flow patterns occur

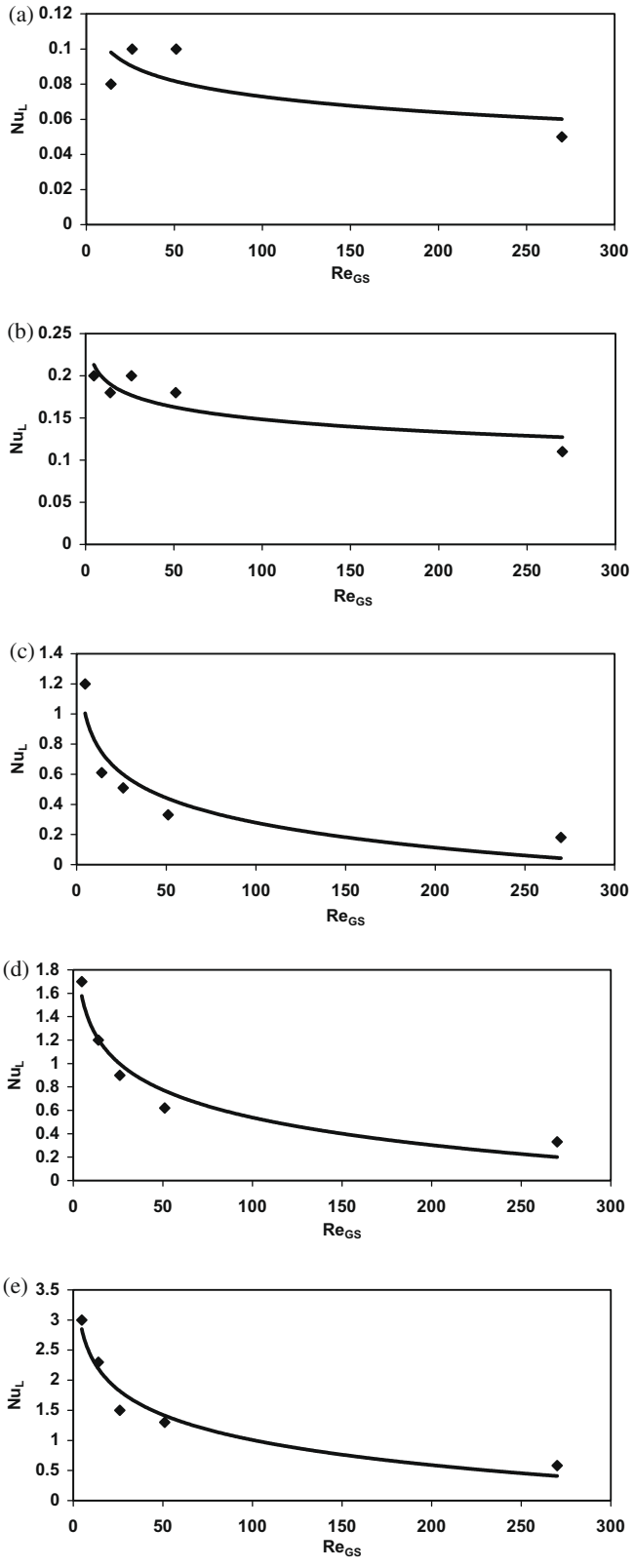

Fig. 10. Effect of superficial gas velocity on heat transfer in parallel triangular micro-channels of d_h = 130 μm: (a) Re_{LS} = 4, (b) Re_{LS} = 8, (c) Re_{LS} = 15, (d) Re_{LS} = 28, (e) Re_{LS} = 56.

simultaneously in different micro-channels. The probability of appearance of different flow patterns should be taken into account for developing flow pattern maps.

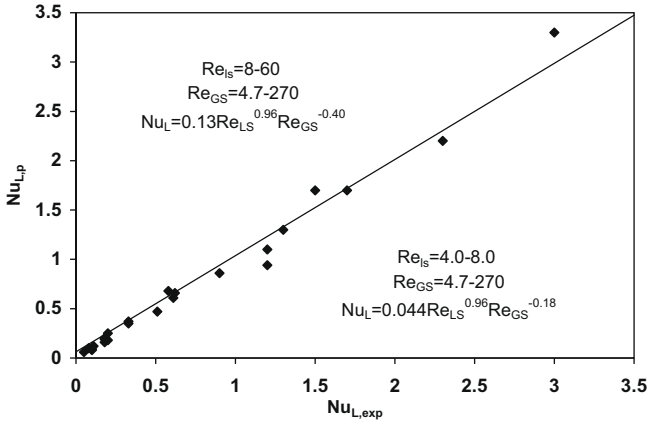

Fig. 11. Comparison of experimental Nusselt numbers to predictions by Eqs. (11) and (12).

Similar void fraction data can be obtained in micro-channels and conventional size channels, but the micro-channel void fraction can be sensitive to the inlet geometry and deviate significantly from the homogeneous flow model. The Lockhart–Martinelli model can correlate the data obtained from pressure drop measurements in gas–liquid flow in parallel micro-channels with hydraulic diameter of 130 μm, the data could be fit by a single value of C = 0.24.

Only a few experimental investigations deal with heat transfer of gas–liquid flow in conventional size channels. There is a significant discrepancy between experimental results on heat transfer presented for channels of d_h = 1–100 mm. No data is available in the literature on gas–liquid heat transfer in micro-channels. Heat transfer in the test section that contains 21 parallel triangular micro-channel of d_h = 130 μm was studied experimentally in the range of superficial velocities U_{LS} = 0.015–0.244 m/s, U_{GS} = 0.50–28.6 m/s. It was shown that the heat transfer coefficient increases with increasing liquid velocity and decreases with increasing air velocity.

Acknowledgement

This research was supported by the Fund for the Promotion of Research at the Technion.

References

[1] S.M. Ghiaasiaan, S.I. Abdel-Khalik, Two-phase flow in micro-channels, Adv. Heat Transfer 34 (2001) 145–254.
[2] A. Serizawa, Z. Feng, Z. Kawara, Two-phase flow in micro-channels, Exp. Thermal Fluid Sci. 26 (2002) 703–714.
[3] A. Kawahara, P.M. Chung, M. Kawaji, Investigation of two-phase flow pattern, void fraction and pressure drop in a micro-channel, Int. J. Multiphase Flow 28 (2002) 411–1435.
[4] S. Garimella, C. Sobhan, Transport in microchannels – a critical review, Ann. Rev. Heat Transfer 13 (2003) 1–50.
[5] G.P. Celata (Ed.), Heat Transfer and Fluid Flow in Micro-channels, Bergel, New York, 2004.
[6] P. Cheng, W.Y. Wu, Mesoscale and microscale phase change heat transfer, in: G. Greene, Y. Cho, J. Hartnett, A. Bar-Cohen (Eds.), Advances in Heat Transfer, 39, Academic, New York, 2006.
[7] G. Hetsroni, B.G. Hu, J.H. Yi, A. Mosyak, L.P. Yarin, G. Ziskind, Heat transfer in intermittent air–water flows: part I, Int. J. Multiphase Flow 24 (2) (1998) 165–188.
[8] G. Hetsroni, B.G. Hu, J.H. Yi, A. Mosyak, L.P. Yarin, G. Ziskind, Heat transfer in intermittent air–water flows: part II, Int. J. Multiphase Flow 24 (2) (1998) 189–212.
[9] G. Hetsroni, D. Mewes, C. Enke, M. Gurevich, A. Mosyak, R. Rozenblit, Heat transfer of two-phase flow in inclined tubes, Int. J. Multiphase Flow 29 (2003) 173–194.
[10] D. Kim, A.J. Ghajar, R.L. Dougherty, V.K. Ryali, Comparison of 20 two-phase heat transfer correlations with seven sets of experimental data, including flow pattern and tube inclination effects, J Heat Transfer Eng 29 (1) (1999) 15–40.

[11] Z.Y. Bao, D.F. Fletcher, B.S. Haynes, An experimental study of gas–liquid flow in a narrow conduit, Int. J. Heat Mass Transfer 43 (2000) 2313–2324.
[12] A.J. Ghajar, J.-Y. Kim, K. Malhotra, S. Trimble, Systematic heat transfer measurements for air–water two-phase flow in horizontal and slightly upward inclined pipe. In: Proceedings of the 10th Brazilian Congress of Thermal Sciences and Engineering – ABCM, Rio de Janeiro 29 (2004) Nov–3 Dec 2004.
[13] R. Zimmerman, M. Gurevich, A. Mosyak, R. Rozenblit, G. Hetsroni, Heat transfer to air–water annular flow in a horizontal pipe, Int. J. Multiphase Flow 32 (2006) 1–19.
[14] G. Hetsroni, A. Mosyak, Z. Segal, E. Pogrebnyak, Two-phase flow patterns in parallel micro-channels, Int. J. Multiphase Flow 29 (2003) 341–360.
[15] K.A. Triplett, S.M. Ghiaasiaan, S.I. Adbel-Khalik, D.L. Sadowski, Gas–liquid two-phase flow in microchannels. Part I: two-phase flow patterns, Int. J. Multiphase Flow 25 (1999) 377–394.
[16] T.S. Zhao, Q.C. Bi, Co-current air–water two-phase flow patterns in vertical triangular microchannels, Int. J. Multiphase Flow 27 (2001) 765–782.
[17] C.A. Damianides, J.W. Westwater, Two-phase flow patterns in a compact heat exchanger and in small tubes. In: Proceedings of the 2nd UK National Conference on Heat Transfer, Glasgow, 14–16 September 1988. Mechanical Engineering, London, 1988, pp. 1257–1268.
[18] T. Fukano, A. Kariyasaki, Characteristics of gas–liquid two-phase flow in a capillary, Nucl. Eng. Des. 141 (1993) 59–68.
[19] K.A. Triplett, S.M. Ghiaasiaan, S.I. Abdel-Khalik, A. LeMouel, McCord BN gas–liquid two-phase flow in microchannels. Part II: void fraction and pressure drop, Int. J. Multiphase Flow 25 (1999) 395–410.
[20] Guide to the Expression of Uncertainty of Measurements, International Organization for Standardisation, Geneva, 1995.
[21] G. Hetsroni, M. Gurevich, A. Mosyak, R. Rozenblit, Surface temperature of a heated capillary-tube by means of an IR technique, Meas. Sci. Tech. 14 (2003) 807–814.
[22] M.I. Ali, M. Sadatomi, M. Kawaji, Two-phase flow in narrow channels between two flat plates, Can. J. Chem. Eng. 71 (1993) 657–666.
[23] A.A. Armand, The resistance during the movement of a two-phase system in horizontal pipes, Izv. Vses. Teplotekh. Inst. 1 (1946) 16–23 (AERE-Lib/Trans 828).
[24] H. Ide, A. Kawahara, M. Kawaji, Comparison of gas–liquid two-phase flow characteristics between min-channels and micro-channels. In: Proceedings of 13th International Heat Transfer Conference, Sydney Convention and Exhibition Centre, Sydney, Australia, 2006, pp. 13–18, August 2006, MPH-51.
[25] R.W. Lockhart, R.C. Martinelli, Proposed correlation of data for isothermal two-phase two-component flow in pipes, Chem. Eng. Prog. 45 (1949) 18–39.
[26] D. Chisholm, Two-phase Flow in Pipelines and Heat Exchangers, Pitman, Bath, England, 1983.
[27] K. Mishima, T. Hibiki, Some characteristics of air–water two-phase flow in small diameter vertical tubes, Int. J. Multiphase Flow 22 (1996) 703–712.